Can coastal upwelling trigger a climate mode? A study on intraseasonal-scale coastal upwelling off Java and the Indian Ocean Dipole

Takanori Horii[1], Eko Siswanto[1], Iskhaq Iskandar[2], Iwao Ueki[1], and Kentaro Ando[3]

[1]Japan Agency for Marine-Earth Science and Technology
[2]University of Sriwijaya
[3]Japan Marine Science and Technology Center(JAMSTEC)

November 22, 2022

Abstract

Coastal upwelling along the southern coast of Java brings cold and nutrient-rich subsurface water to the surface. We explored whether the upwelling could trigger the onset of the Indian Ocean Dipole (IOD) by supplying cold water to the southeastern tropical Indian Ocean. We used satellite-based daily chlorophyll-a concentration (Chl-a) data during 2003-2020 as a proxy of the coastal upwelling. We focused on first Ch-a blooming that occurred in April–June, the onset phase of the positive IOD (pIOD). We found that the timing and strength of the upwelling signals were significantly correlated with the subsequent IOD peaks. We diagnosed processes associated with the upwelling affecting sea surface temperature (SST) in the southeastern Indian Ocean. Results indicate that after the cold-water upwelling south of Java, westward surface temperature advection plays a role in anomalously cooling the SST in the southeastern Indian Ocean and setting a favorable condition for the subsequent pIOD development.

Can coastal upwelling trigger a climate mode? A study on intraseasonal-scale coastal upwelling off Java and the Indian Ocean Dipole

T. Horii[1], E. Siswanto[2], I. Iskandar[3], I. Ueki[1] and K. Ando[1]

[1]Global Ocean Observation Research Center, Research Institute for Global Change, Japan Agency for Marine-Earth Science and Technology, 2-15, Natsushima, Yokosuka, Kanagawa 237-0061 Japan

[2]Earth Surface System Research Center, Research Institute for Global Change, Japan Agency for Marine-Earth Science and Technology, 3173-25, Showa-machi, Kanazawa-ku, Yokohama, Kanagawa 236-0001, Japan

[3]Faculty of Mathematics and Natural Sciences, Sriwijaya University, Jl. Masjid Al Gazali, Bukit Lama, Palembang 30128, Indonesia

Corresponding author: Takanori Horii (horiit@jamstec.go.jp)

Horii, Takanori (ORCID ID: 0000-0003-2044-4226)
Siswanto, Eko (ORCID ID: 0000-0002-8215-0082)
Iskandar, Iskhaq (ORCID ID: 0000-0002-9253-4821)
Ueki, Iwao (ORCID ID: 0000-0002-8760-2666)
Ando, Kentaro (ORCID ID: 0000-0003-1924-3910)

Key Points

- Satellite-based surface chlorophyll-a (Chl-a) can be a proxy of intraseasonal-scale coastal upwelling along the southern coast of Java.
- The timing and strength of the upwelling signals were significantly correlated with the subsequent peak of the Indian Ocean Dipole (IOD).
- The coastal upwelling may contribute to the onset and development of positive IOD through the process of anomalous cold-water advection.

Abstract

Coastal upwelling along the southern coast of Java brings cold and nutrient-rich subsurface water to the surface. We explored whether the upwelling could trigger the onset of the Indian Ocean Dipole (IOD) by supplying cold water to the southeastern tropical Indian Ocean. We used satellite-based daily chlorophyll-a concentration (Chl-a) data during 2003-2020 as a proxy of the coastal upwelling. We focused on first Ch-a blooming that occurred in April–June, the onset phase of the positive IOD (pIOD). We found that the timing and strength of the upwelling signals were significantly correlated with the subsequent IOD peaks. We diagnosed processes associated with the upwelling affecting sea surface temperature (SST) in the southeastern Indian Ocean. Results indicate that after the cold-water upwelling south of Java, westward surface temperature advection plays a role in anomalously cooling the SST in the southeastern Indian Ocean and setting a favorable condition for the subsequent pIOD development.

Plain Language Summary

Along the southwestern coastal waters of Java islands in Indonesia, coastal upwelling brings up cold water from below and can cool the ocean surface temperatures. Past studies reported that strong upwelling signals were observed together with the positive Indian Ocean Dipole (IOD) phenomenon. However, it was unclear if and how the coastal cold water spreads over large area of the Indian Ocean and affect the occurrence of IOD. We used sea surface chlorophyll-a (Chl-a) data estimated from satellite observations as an indicator of coastal upwelling. We focused on the date when the first Chl-a blooming occurred south of Java in each year. On average, Chl-a blooming occurs around June, but in years when it occurred earlier (around April-May), Chl-a blooming was followed by a positive IOD event in August-October. We further investigated how the cold water in the coastal area spreads widely over the eastern Indian Ocean. It was found that stronger westward ocean currents expanded the cold water to a wider area of the eastern Indian Ocean and can set a favorable condition for the development of the positive IOD. Thus, accurate observation and understanding of the coastal upwelling may improve the predictability of the Indian Ocean climate.

1 Introduction

The Indian Ocean Dipole (IOD) is a climate mode in the Indian Ocean (Saji et al., 1999) that is characterized by the development of basin-wide dipole pattern in the anomalous sea surface temperature (SST). The large-scale SST change causes a shift in the atmospheric circulations and affects the global climate (e.g., Saji and Yamagata, 2003) and causes extreme weather conditions such as flooding in east Africa (Black et al., 2003) and droughts in east Australia (Ummenhofer et al., 2009). A more detailed understanding of the onset and development of the IOD, as well as its earlier prediction, is an important issue in an Indian Ocean climate study.

In the onset phase of a positive IOD (pIOD) event, cold SST anomalies (SSTA) with anomalous southeasterly winds first appear off the coasts of Sumatra and Java around April−May (Saji et al., 1999; Susanto et al., 2001; Xie et al., 2002). The cold SSTA then spread in the southeastern tropical Indian Ocean and the warm SSTA spread in the west due to coupled ocean-atmosphere interactions. From a large-scale perspective, the initial SST signal indicates the result that large-scale changes in the atmosphere and ocean associated with the IOD, i.e., anomalous winds and subsurface conditions in the tropical Indian Ocean, are exposed as enhanced seasonal coastal upwelling along the Indonesian coasts (e.g., Xie et al., 2002).

Various factors can set up a favorable background condition for the onset of the pIOD, such as the El Niño-Southern Oscillation (ENSO) (e.g., Annamalai et al., 2003), biennial monsoon variability in the Indian Ocean (Crétat et al., 2018), and anomalous oceanic and atmospheric condition in the southern Indian Ocean (Fischer et al., 2005; Zhang et al., 2020). Based on these previous achievements, the present study focuses on the coastal upwelling along the southern coast of Java (e.g., Wyrtki, 1962; Susanto et al., 2001), the spatial scale of which is one to two orders smaller than these large-scale factors. Could the coastal upwelling actively contribute to the onset and development of pIOD events, not only as a dependent variation of the large-scale air-sea coupled interaction associated with the IOD? This hypothesis is based on the expansion of cold SSTA from off Sumatra and Java to the southeastern Indian Ocean from May to August observed by satellite and in-situ moored buoy data (Vinayachandran et al., 2007; Horii et al., 2008; 2009) during the 2006 pIOD.

On the cold SSTA south of Java, Delman et al. (2016) pointed out that the cooling around May-July was a precursor of a pIOD which is driven by upwelling Kelvin waves. While several studies used numerical models and investigated the ocean temperature variations along the coasts of Sumatra and Java associated with IOD (Du et al., 2008; Halkides and Lee, 2009; Delman et al., 2018), no observational study has focused on the onset phase of the IOD and quantified the possible contribution of the coastal upwelling to SST variations over the eastern Indian Ocean. We explore the possibility that the anomalous cold water along the coasts leads to subsequent large-scale IOD onset and development. If this possibility holds, understanding the coastal upwelling in the southeastern Indian Ocean could contribute to a better understanding of the IOD and thus a better prediction.

To clarify the coastal upwelling variations around May−June, we need to resolve intraseasonal-scale variations. Past studies showed that there is a short-term occurrence of the upwelling due to anomalous southeasterly alongshore winds (Chen et al., 2015; Horii et al., 2016; Cao et al., 2019) during a certain phase of intraseasonal (approximately 20- to 50-day) variation, referred to as Madden-Julian oscillation (MJO) (Madden and Julian 1994) or

intraseasonal oscillation (ISO) (Lawrence and Webster, 2002). However, compared to the open ocean (e.g., McPhaden et al., 2009), there have been fewer such hydrographic timeseries in the coastal area. Analyses by satellite-observed SST (e.g., Hendiarti et al., 2004) or daily sea level variations (Horii et al., 2016; 2018) cannot necessarily discriminate the SST cooling due to coastal upwelling. Satellite-based Chl-a data could be a proxy for the coastal upwelling, but because of the large missing values, most previous studies used monthly averages (e.g., Susanto and Marra, 2005; Iskandar et al., 2009). Recently, Xu et al. (2021) used daily-interpolated data and outlined the intraseasonal and interannual surface Chl-a variations in the southeastern Indian Ocean.

The present study makes daily timeseries for the coastal upwelling signals based on the satellite-based Chl-a data. We herein primarily report relationships on the coastal upwelling signal in the onset phase of the IOD and its subsequent evolution. We also diagnose the process of how and to what extent the coastal upwelling can contribute to the SSTA variation in the southeastern Indian Ocean.

2 Data and processing

2.1. A proxy of the coastal upwelling

To make a proxy of the coastal upwelling south of Java, we used daily merged surface Chl-a data (OCEANCOLOUR_GLO_CHL_L3_REP_OBSERVATIONS_009_085) provided by the Copernicus Marine Service (Garnesson et al., 2019). The original grids are 1/24°×1/24° grids (approximately 4.6 km). This product is based on a multiple ocean color sensors but is limited to daily observations, i.e., not applied a space-time interpolation. Due to the large number of missing values off Sumatra, we focused on the region south of Java, where the missing values were relatively small. We analyzed the period from 2003 to 2020 during which the moderate resolution imaging spectroradiometer (MODIS) is incorporated into the merged data.

As a proxy of the coastal upwelling, the average Chl-a data south of Java was computed as follows. (1) A spatial Gaussian filter with an e-folding scale of 1/4° was applied to the original Chl-a dataset to produce data with 1/8°×1/8° grids. Here, the data was calculated only if there were more than 50% data around each grid. (2) A temporal linear interpolation was applied for a missing period within four days. These procedures can be applicable here because we focus on time scales more than intraseasonal variability (> 20 days) while ignoring ocean sub-mesoscale disturbances. We confirmed that the results did not change even if we traded the order of the (1) and (2) above. (3) The interpolated Chl-a data are averaged over the coastal region (Figures 1 and S1), defined as inside the line between (8.0°S, 106°E) and (9.5°S, 114°E), which is approximately 100 km from the Java coast. The spatial scale is appropriate for observing the coastal upwelling signals (Horii et al., 2018). After (1) and (2), available data in the region during April–September in each year was 91.5% on average, and ranged from 75.6% (2010) to 99.7% (2019) (Table S1). Finally, we estimated the error range using a statistical method. See the Supporting Information (Text S1 and Figure S2) for details. The error ranges are shown in Figure S3.

To estimate the thermocline variation south of Java, we used hourly sea level data from a tidal station (7.75°S, 109.02°E) along the coast (Figure S1). Following the procedure of Horii et al. (2016), we prepared a daily sea level anomaly (SLA) timeseries with barometric corrections

and tides removed. We also used SST data provided by the National Oceanic and Atmospheric Administration (NOAA) daily optimum interpolation (OI) SST dataset (Reynolds et al., 2007).

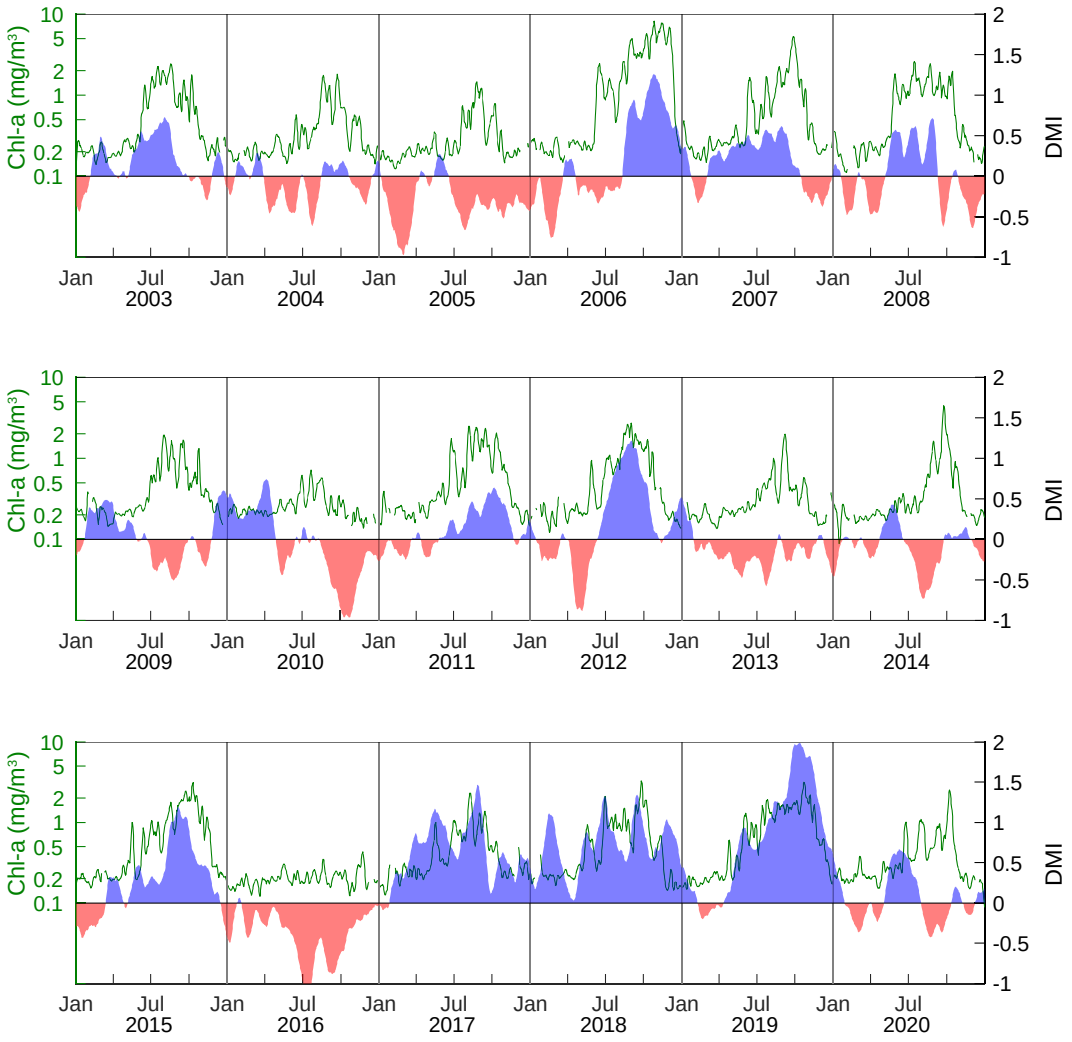

Figure 1. Timeseries of Chl-a concentration (mg/m^3; left axis; logscale) averaged south of Java (see Figure S1 for the map). The light blue and red shades indicate timeseries of 31-day running-mean Dipole Mode Index (DMI; right axis).

2.2. Comparison to SST and sea level variations

The first peaks of Chl-a from April to August in each year were mostly accompanied by SST cooling and lowering of SLA (Figures 2 and S2). Based on our previous study, the lowering SLA is consistent with the shoaling thermocline south of Java (Horii et al., 2018). For example, the Chl-a peaks (> 2.0 mg/m^3) in mid-June in 2006 and 2007 were concurrent with SST cooling and SLA lowering (Figure S3). We defined the first significant Chl-a signal in each year based on the double standard deviations (STD) of Chl-a variability from April to June (0.45). Based on the first signals, we made a composite timeseries of temporal changes in SSTA and SLA (Figure

159 2). The average peaks of the SST cooling and SLA lowering were approximately −3.7
160 (°C/month) and −39 (cm/month), respectively, and these signals are statistically significant at the
161 90% level. Significant lowering in SLA first appeared from day −16, and then SST cooling and
162 Chl-a increase occur concurrently. We conclude that coastal upwelling signals south of Java can
163 be observed from the Chl-a proxy during the onset phase of the IOD.

164

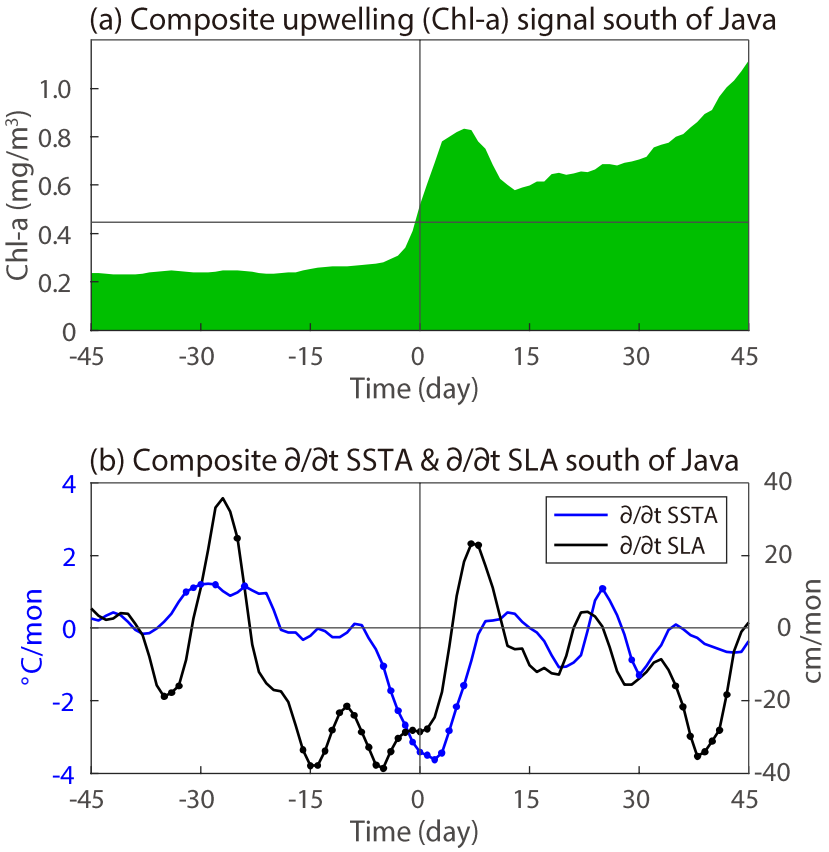

165

166 **Figure 2**. (a) Composite timeseries of Chl-a south of Java from day −45 to +45 based on the first
167 Chl-a blooming during 2003–2020 (Table S1). (b) As in (a), but for temporal changes in sea
168 surface temperature anomalies (SSTA) (blue;°C/month) and sea level anomaly (SLA) (black;
169 cm/month) south of Java. The SSTA was averaged in the same region as the Chl-a. Five-day
170 running mean filters were applied. The values with dots are statistically significant at the 90%
171 level.

172

173 2.3. Other datasets

174 The daily sea surface wind dataset was obtained from the product of the ASCAT satellite.
175 To diagnose the ocean surface heat advection, we used the Ocean Surface Current Analysis-Real
176 Time (OSCAR) data (Bonjean and Largerloef, 2002). To investigate surface heat flux variation,
177 we used the TropFlux dataset (Praveen Kumar et al., 2012). We also used monthly Chl-a data
178 from the Sea-viewing Wide-Field of view Sensor (SeaWiFS) for 1998-2007 to observe the
179 climatology. Using the OI SST mentioned above, we calculated Dipole Mode Index (DMI; Saji

et al., 1999) as the difference in SSTA between western (50°E–70°E, 10°S–10°N) and eastern regions (90°E–110°E, 10°S–0°).

3 Coastal upwelling signals and subsequent IOD events

The daily Chl-a timeseries for the coastal region south of Java, the proxy of the coastal upwelling, shows weak variations from December to March and has seasonal peaks from August to October in most years (Figure 1). The development and peak of Chl-a are concurrent with southeasterly monsoon winds over the southeastern Indian Ocean. The year-to-year variations show that the Chl-a signals are generally larger in pIOD years such as 2006 and 2019, while the signals are smaller in negative IOD (nIOD) years such as 2010 and 2016. In several pIOD years (Table S1), significant intraseasonal-scale Chl-a signals above 0.5 mg/m^3 appeared in April−June, earlier than the seasonal coastal upwelling period in July−October. This indicates an early supply of cold water due to a short-term upwelling from April to early June in these years.

We focused on the earlier coastal upwelling signals than the basin-scale SSTA developments in several pIOD years (Figure 1) and investigated the relationship between the timing of the first Chl-a signal and the subsequent IOD condition in each year (Figure 3a). A daily timeseries enabled us to observe a significant correlation between the timing of the first upwelling signals and the subsequent IOD peaks: coastal upwelling signals before early-June tended to be followed by pIOD events with DMI>0.5. On the other hand, in neutral years and nIOD years, most of the coastal upwelling signals occurred after mid-June. Most of the first Chl-a bloomings are significant, even when taking into account the error ranges (Figure S3). Note that the result did not change when the threshold of 2STD was replaced from 3STD to 5STD, whereas this relationship did not hold for 1STD because a sporadic weak Chl-a signal was detected in January–March.

We also investigated the relationship between the Chl-a amplitude observed in April–June and the subsequent IOD condition (Figure 3b). The Chl-a averaged in April–June was significantly correlated with the subsequent DMI peaks. The average Chl-a signals greater than 0.4 mg/m^3 during April–June were followed by pIOD events. On the other hand, pIOD events did not develop when the average Chl-a was less than 0.35 mg/m^3, except in 2012. Among 10 pIOD cases (blue), no significant relationship was obtained between the preceding Chl-a signal and the subsequent DMI peaks. The results did not change with the minor modification of the averaged period of Chl-a or for the case in which we used the average DMI around the peaks (August–October).

To determine whether the coastal upwelling signals depend on the large-scale ocean-atmosphere condition, we also checked the correlation between the average Chl-a (April–June) and the Nino-3.4 index or DMI in the same period. The correlation between Chl-a and Nino-3.4 was −0.30, whereas that with DMI was +0.44. This suggests that in the onset phase of the IOD (April–June), it is unlikely that the coastal upwelling signals occurred due to the large-scale change of the tropical Pacific and Indian Ocean associated with ENSO and IOD, respectively. The Chl-a signals in April–June were concurrent with intraseasonal-scale local SST and SLA variations (Figure S3).

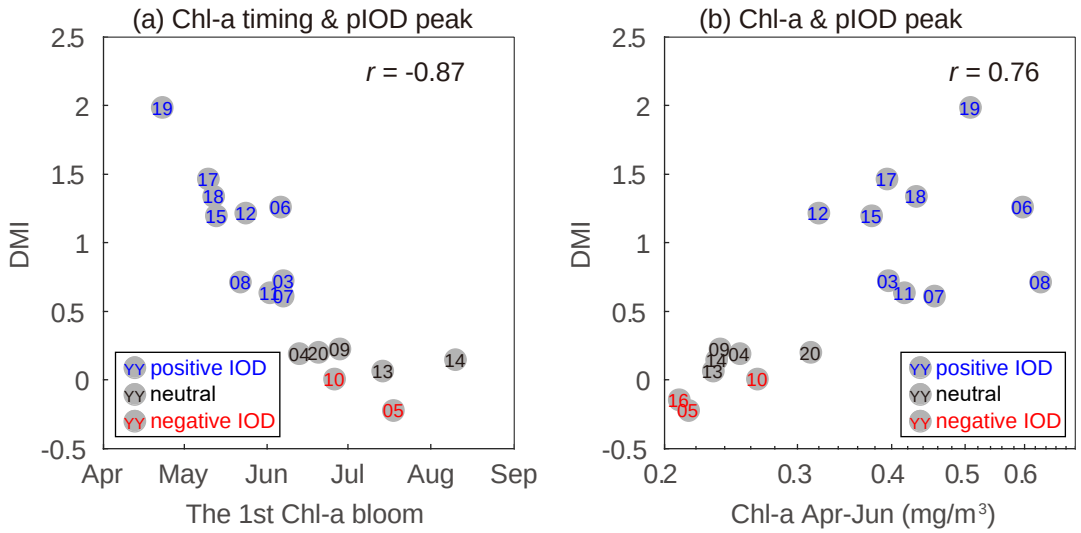

Figure 3. (a) Scatterplot between the timing of the first Chl-a blooming and subsequent maximum DMI during August–October. (b) As in (a), but for the average Chl-a from April to June. The numerals denote the year (e.g., '06' means '2006'). The correlation coefficient (*r*) is shown in each panel.

4 Anomalous surface temperature advection associated with the coastal upwelling

To investigate whether and to what extent the early occurrence of the coastal upwelling plays a role to anomalously cool the SST in the eastern Indian Ocean, we observe composite SSTA (Figure 4) based on the first Chl-a signal in each year (Table S1 and Figure S3). After the upwelling around April–June in pIOD years, significant cold SSTA develop in the southeastern Indian Ocean, including the coastal regions (Figure 4a). The largest cooling is observed south of Java, reaching −1.5°C in one month. The wider distribution of the cold SSTA than the spatial scale of the coastal upwelling is due to the surface heat flux variation. The period (day 0 to approximately +30) follows the easterly phase of the ISO in which the stronger southeasterly alongshore winds enhanced the latent surface heat cooling there (Horii et al., 2016; Cao et al., 2019). For the upwelling in other years, the development of the cold SSTA south of Java is similar to that in pIOD years, although the cooling is confined south of Java, whereas anomalous SST warming is also observed in the west of 100°E.

To diagnose the processes on the expanded cold SSTA observed in the onset phase of the pIOD, we investigate the contribution of anomalous cold-water advection. Anomalous advections are expected to be due to offshore-ward Ekman flow driven by alongshore southeasterly wind anomalies (Wirasatriya et al., 2020) and enhanced northwestward south Java currents (Quadfasel and Cresswell, 1992). Using observational datasets, we estimated the anomalous surface temperature advections. The horizontal mixed-layer temperature gradient and surface currents were estimated using the SST and OSCAR dataset, respectively. See the Supporting Information (Text S2) for details. Although the estimated horizontal temperature advection contains errors of approximately 0.5°C/month in the southeastern Indian Ocean (Horii et al., 2009), it is useful to diagnose SST variations associated with IOD (Horii et al., 2013). We

also diagnosed the contribution of surface heat flux variations, assuming a mixed layer depth of 30 m.

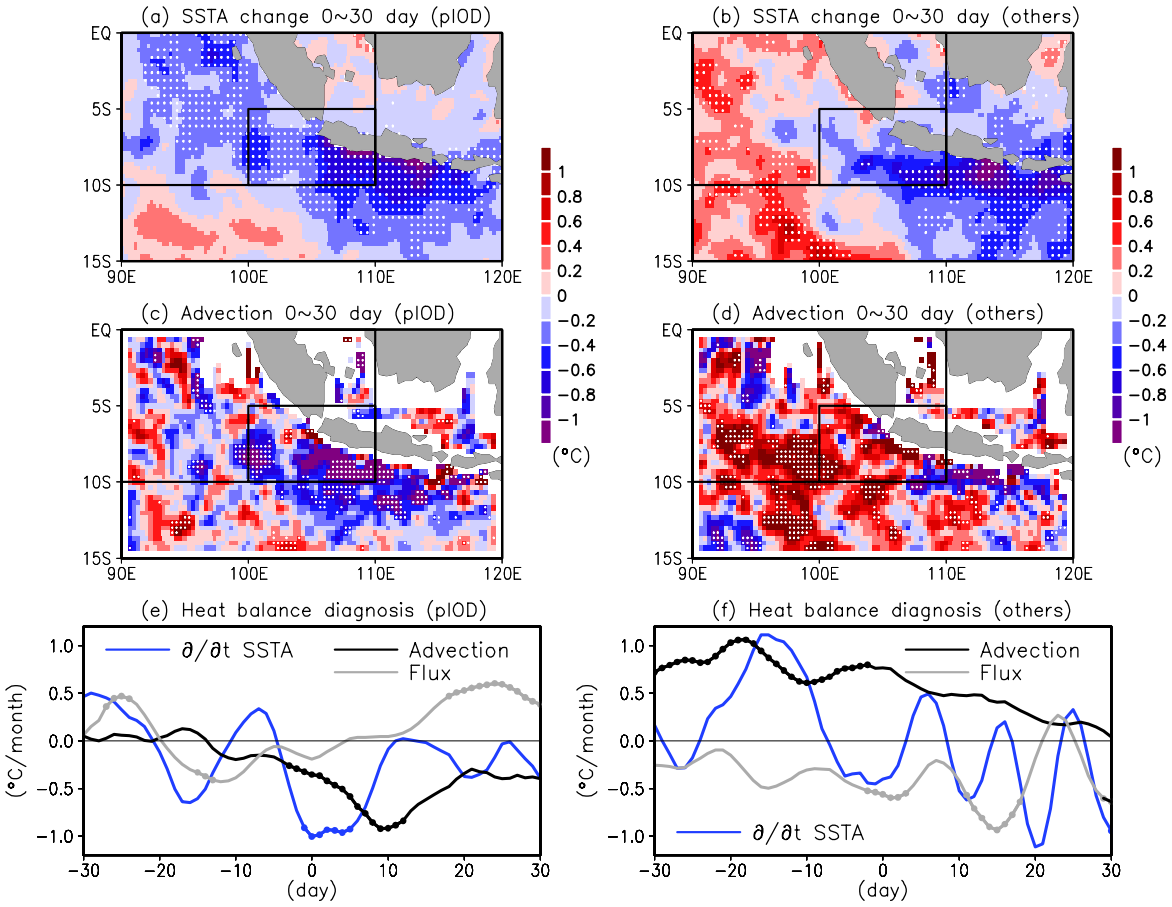

Figure 4. Composite SSTA change (°C) from day 0 to day +30 based on the first upwelling signal for (a) 10 pIOD years and (b) 7 other years. (c) and (d) As in (a) and (b), but for horizontal surface temperature advection anomalies integrated from day 0 to day +30, respectively. (e) Composite timeseries for 10 pIOD years for the area (100°E–110°E, 10°S–0°) shown in Figure 4a–d. The lines denote the temporal change in the SSTA (blue), the surface horizontal temperature advection (black), and the contribution of net surface heat flux (gray). Positive heat flux indicates a heat gain for the ocean. (f) As in (e), but for 7 other years. The values with dots are statistically significant at the 90% level.

After the first signal of coastal upwelling in pIOD years, significant cold temperature advection anomalies extend westward from the coastal region to the open ocean. The regional peak around 10°–7°S, 98°–103°E is consistent with that in the SSTA change. The anomalous cold advection is primarily explained by the nonlinear zonal advection (Text S2 and Figure S4). Anomalously enhanced westward surface currents bring cold temperature anomalies from east to west. The pair of climatological (anomalous) westward currents and anomalous (climatological) temperature gradients also has a secondary role in the cooling (Figure S4). On the other hand,

cold advection anomalies were observed only south of Java for other years and warm advection anomalies were prominent west of 107°E (Figure 4d).

We diagnose the anomalous contribution of the surface heat flux and horizontal temperature advection to SSTA changes before and after the coastal upwelling signals for the southeastern sector (100°E–110°E, 10°S–5°S) of the eastern pole of the IOD. The flux contribution was estimated by the net surface heat flux. On the composite of pIOD years, SSTA changes and advection anomalies have similar amplitudes and show significant cooling from day −1 to day +5 and from day −3 to day +12, respectively (Figure 4e). The flux occasionally contributes to the cooling around day −15, but shows warming after day +18. The total flux does not contribute to cooling in the region. Neither surface heat flux nor advection explains the peak SSTA cooling around day 0. Ocean vertical processes that are not quantified here must play a role in the cooling. Nevertheless, the integrated contribution from the advection for one month after the first coastal upwelling signal (day 0) is −0.8°C and is equivalent to the observed SSTA change (−1.0°C). On the other hand, there are no significant SSTA changes in the composite timeseries for other years (Figure 4f), as the timing of SSTA cooling varies among the cases. From day −30 to day −2, anomalous warm advections from the west due to eastward surface current anomalies significantly contribute to the warming. Unlike pIOD years, anomalous heat flux mainly by the enhanced latent heat flux significantly contributes to the temperature change of −0.5°C to −1.0°C with peaks at day 0 and day +15.

These results indicate that intraseasonal-scale coastal upwelling around April to early June in pIOD years leads to SSTA cooling in the southeastern Indian Ocean on a temporal scale approximately one month thereafter. This anomalous cold advection prevails only in the pIOD years when an earlier occurrence of the anomalously cold coastal waters is effectively expanded to the open ocean in the form of nonlinear advection anomalies. Implications of the cooling for the IOD onset and development are further discussed in the next section.

5 Discussion and conclusions

A daily proxy of the coastal upwelling south of Java showed some relationships between the early occurrence of the upwelling and the subsequent IOD evolution (Figure 3). Anomalous cold advections to the open ocean associated with the coastal upwelling in pIOD years were also demonstrated (Figure 4). Further question should be how this signal could promote the development of the basin-scale IOD. An earlier supply of cold temperature anomalies into the eastern edge of the tropical Indian Ocean may have an implication for triggering ocean-atmosphere interaction. Since the climatological SST in the eastern equatorial Indian Ocean has its peak in April–May, the cold SSTA south of Java appearing in this period results in a large SST gradient with a spatial scale of approximately 1,000 to 2,000 km. This large SST gradient can provide a favorable condition for Bjerknes feedback, which is essential for the development of the IOD.

The SST cooling by the anomalous cold advections in the southeastern Indian Ocean is observed only in the pIOD years, whereas intraseasonal-scale coastal upwelling signals are present in most years (e.g., Cao et al., 2019). This indicates that the background conditions in the eastern Indian Ocean around April–May are essential for the onset and development of the IOD (e.g., Song et al., 2008). The present study suggests that it would be important to have

intraseasonal-scale coastal upwelling under the condition of a shallow thermocline in the eastern Indian Ocean. This leads to subsequent anomalous coolings that expand over a wider area due to nonlinear cold advection anomalies. Note that in some years, large-scale dipole SSTA (pIOD) have already appeared before the first upwelling signals, such as in 2007, 2017, and 2018 (Figure 1). In these cases, the basin-scale SSTA and atmosphere-ocean interaction started by surface heat flux (e.g., Wang et al., 2020), and the coastal upwelling plays a secondary role in further cooling the SSTA. Further studies including the use of numerical models are needed to better quantify the coastal upwelling and its potential impact on IOD onset.

Finally, we would like to note that the relationship between the coastal upwelling south of Java and the subsequent pIOD is similar to that between westerly wind bursts (WWB) and subsequent El Niño in the tropical Pacific, although these are opposite anomalous conditions. Both climate modes develop due to intraseasonal-scale forcing on favorable background fields. Thus, understanding the coastal upwelling signals will help predict pIOD events as well as WWB on El Niño events. We recognize that appropriate observation of the eastern boundary region in the tropical Indian Ocean will contribute to Indian Ocean climate study.

Open Research

Merged surface Chl-a concentration data were provided by the Copernicus Marine Service (https://resources.marine.copernicus.eu/product-detail/OCEANCOLOUR_GLO_CHL_L3_REP_OBSERVATIONS_009_085/DATA-ACCESS). Monthly Chl-a data from Sea-viewing Wide Field-of-view Sensor (SeaWiFS) were provided by the Goddard Space Flight Center of NASA and were obtained through the Asia-Pacific Data-Research Center (APDRC; http://apdrc.soest.hawaii.edu/datadoc/seawif_v5.2_mon.php). Quality-controlled sea level data from tide gauges were provided by the University of Hawaii Sea Level Center (https://uhslc.soest.hawaii.edu/opendap/rqds/global/hourly/contents.html). Optimum interpolation SST data were provided by NOAA (https://psl.noaa.gov/data/gridded/data.noaa.oisst.v2.highres.html). Wind data of the ASCAT satellite were provided by the Centre de Recherche et d'Exploitation Satellitaire (CERSAT) at IFREMER and were obtained through APDRC (http://apdrc.soest.hawaii.edu/datadoc/ascat.php). Ocean surface current data (OSCAR) were provided by Physical Oceanography Distributed Active Archive Center at the Jet Propulsion Laboratory of NASA (https://podaac.jpl.nasa.gov/dataset/OSCAR_L4_OC_third-deg). Air-sea flux data (TropFlux dataset) were provided by the Indian National Centre for Ocean Information Services (https://incois.gov.in/tropflux/data_access.jsp).

Acknowledgments

The present study was supported by the Japan Society for the Promotion of Science (JSPS) Grants-in-Aid for Scientific Research, 18K03753 and 18H03731.

References

Annamalai, H., Murtugudde, R., Potemra, J., Xie, S.-P., Liu, P., and Wang, B. (2003). Coupled dynamics over the Indian Ocean: spring initiation of the Zonal Mode, Deep Sea Research Part II, 50(12-13), 2305-2330.

Black, E., Slingo, J., and Sperber, K. R. (2003). An observational study of the relationship between excessively strong short rains in coastal East Africa and Indian Ocean SST. Monthly Weather Review, 131(1), 74-94.

Cao, G., Xu, T., He, Y., Wang, L., Wang, D., Wei, Z., and Zhu, Y. (2019). Seasonality in intraseasonal sea surface temperature variability along the Sumatra-Java southern coast. Journal of Geophysical Research: Oceans, 124. https://doi.org/10.1029/2018JC014853

Chen, G., Han, W., Li, Y., Wang, D., and Shinoda, T. (2015). Intraseasonal variability of upwelling in the equatorial Eastern Indian Ocean. Journal of Geophysical Research: Oceans, 120, 7598–7615. https://doi.org/10.1002/2015JC011223

Crétat, J., Terray, P., Masson, S., and Sooraj, K. P. (2018). Intrinsic precursors and timescale of the tropical Indian Ocean Dipole: insights from partially decoupled numerical experiment. Climate Dynamics, 51(4), 1311-1332.

Delman, A. S., Sprintall, J., McClean, J. L., and Talley, L. D. (2016). Anomalous Java cooling at the initiation of positive Indian Ocean Dipole events. Journal of Geophysical Research: Oceans, 121, 5805–5824. https://doi.org/10.1002/2016JC011635

Delman, A. S., McClean, J. L., Sprintall, J., Talley, L. D., and Bryan, F. O. (2018). Process-specific contributions to anomalous Java mixed layer cooling during positive IOD events. Journal of Geophysical Research: Oceans, 123. https://doi.org/10.1029/2017JC01374

Du, Y., Qu, T., and Meyers, G. (2008). Interannual variability of sea surface temperature off Java and Sumatra in a global GCM. Journal of Climate, 21(11), 2451-2465.

Fischer, A. S., Terray, P., Guilyardi, E., Gualdi, S., and Delecluse, P. (2005). Two independent triggers for the Indian Ocean dipole/zonal mode in a coupled GCM. Journal of Climate, 18(17), 3428-3449.

Garnesson, P., Mangin, A., Fanton d'Andon, O., Demaria, J., and Bretagnon, M. (2019). The CMEMS GlobColour chlorophyll a product based on satellite observation: Multi-sensor merging and flagging strategies. Ocean Science, 15(3), 819-830. https://doi.org/10.5194/os-15-819-2019

Halkides, D. J., and Lee, T. (2009). Mechanisms controlling seasonal-to-interannual mixed layer temperature variability in the southeastern tropical Indian Ocean. Journal of Geophysical Research: Oceans, 114(C2).

Hendiarti, N., Siegel, H., and Ohde, T. (2004). Investigation of different coastal processes in Indonesian waters using SeaWiFS data. Deep Sea Research Part II: Topical Studies in Oceanography, 51(1-3), 85-97.

Horii, T., Hase, H., Ueki, I., and Masumoto, Y. (2008). Oceanic precondition and evolution of the 2006 Indian Ocean dipole. Geophysical Research Letters, 35(3).

Horii, T., Masumoto, Y., Ueki, I., Hase, H., and Mizuno, K. (2009). Mixed layer temperature balance in the eastern Indian Ocean during the 2006 Indian Ocean dipole. Journal of Geophysical Research: Oceans, 114(C7).

Horii, T., Ueki, I., Ando, K., and Mizuno, K. (2013). Eastern Indian Ocean warming associated with the negative Indian Ocean dipole: A case study of the 2010 event. Journal of Geophysical Research: Oceans, 118(1), 536-549. doi:10.1002/jgrc.20071.

Horii, T., Ueki, I., Syamsudin, F., Sofian, I., and Ando, K. (2016). Intraseasonal coastal upwelling signal along the southern coast of Java observed using Indonesian tidal station data. Journal of Geophysical Research: Oceans, 121, 2690– 2708. https://doi.org/10.1002/2015JC010886

Horii, T., Ueki, I., and Ando, K. (2018). Coastal upwelling events along the southern coast of Java during the 2008 positive Indian Ocean Dipole. Journal of Oceanography 74 (5), 499–508, doi: 10.1007/s10872-018-0475-z.

Iskandar, I., Rao, S. A., and Tozuka, T. (2009). Chlorophyll-a bloom along the southern coasts of Java and Sumatra during 2006. International Journal of Remote Sensing, 30(3), 663-671.

Lawrence, D. M., and Webster, P. J. (2002). The boreal summer intraseasonal oscillation: Relationship between northward and eastward movement of convection. Journal of Atmospheric Science, 59, 1593–1606.

Madden R. A., and Julian, P. R. (1994) Observations of the 40-50 day tropical oscillation: a review. Monthly Weather Review, 122, 814–837

McPhaden, M. J., Meyers, G., Ando, K., Masumoto, Y., Murty, V. S. N., Ravichandran, M., Syamsudin, F., Vialard, J., Yu, L., and Yu, W. (2009). RAMA: the research moored array for African–Asian–Australian monsoon analysis and prediction. Bulletin of the American Meteorological Society, 90(4), 459-480.

Praveen Kumar, B., Vialard, J., Lengaigne, M., Murty, V., and McPhaden, M. J. (2012). Tropflux: Air-sea fluxes for the global tropical oceans description and evaluation. Climate Dynamics, 38, 1521–1543. doi:10.1007/s00382-012-1455-4.

Quadfasel, D., and Cresswell, G. R. (1992). A note on the seasonal variability of the South Java Current. Journal of Geophysical Research: Oceans, 97(C3), 3685-3688.

Reynolds, R. W., Smith, T. M., Liu, C., Chelton, D. B., Casey, K. S., and Schlax, M. G. (2007). Daily high-resolution-blended analyses for Sea Surface Temperature. Journal of Climate, 20, 5473–5496. https://doi.org/10.1175/2007JCLI1824.1

Saji, N. H., Goswami, B. N., Vinayachandran, P. N., and Yamagata, T. (1999). A dipole mode in the tropical Indian Ocean. Nature, 401(6751), 360-363.

Saji, N. H., and Yamagata, T. J. C. R. (2003). Possible impacts of Indian Ocean dipole mode events on global climate. Climate Research, 25(2), 151-169.

Song, Q., Vecchi, G. A., and Rosati, A. J. (2008). Predictability of the Indian Ocean sea surface temperature anomalies in the GFDL coupled model. Geophysical research letters, 35(2).

Susanto, R. D., Gordon, A. L., and Zheng, Q. (2001). Upwelling along the coasts of Java and Sumatra and its relation to ENSO. Geophysical Research Letters, 28(8), 1599-1602.

Susanto, R. D., and J. Marra (2005), Effects of the 1997/98 El Niño on Chlorophyll a variability along the southern coasts of Java and Sumatra, Oceanography, 18(4), 124–127, doi:10.5670/oceanog.2005.13.

Ummenhofer, C. C., England, M. H., McIntosh, P. C., Meyers, G. A., Pook, M. J., Risbey, J. S., Gupta, A. S., and Taschetto, A. S. (2009). What causes southeast Australia's worst droughts? Geophysical Research Letters, 36(4), 36, L04706, doi:10.1029/2008GL036801.

Vinayachandran, P. N., Kurian, J., and Neema, C. P. (2007). Indian Ocean response to anomalous conditions in 2006. Geophysical Research Letters, 34(L15602), 1-6.

Wang, G., Cai, W., Yang, K., Santoso, A., and Yamagata, T. (2020). A unique feature of the 2019 extreme positive Indian Ocean Dipole event. Geophysical Research Letters, 47, e2020GL088615. https://doi.org/10.1029/2020GL088615.

Wirasatriya, A., Setiawan, J. D., Sugianto, D. N., Rosyadi, I. A., Haryadi, H., Winarso, G., Setiawan, R. Y., and Susanto, R. D. (2020). Ekman dynamics variability along the southern coast of Java revealed by satellite data, International Journal of Remote Sensing, 41 (21), 8475-8496.

Wyrtki, K. (1962). The upwelling in the region between Java and Australia during the south-east monsoon. Australian Journal of Marine and Freshwater Research, 13, 217–225.

Xie, S. P., Annamalai, H., Schott, F. A., and McCreary Jr., J. P. (2002). Structure and mechanisms of South Indian Ocean climate variability. Journal of Climate, 15(8), 864-878.

Xu, T., Wei, Z., Li, S., Susanto, R. D., Radiarta, N., Yuan, C., Setiawan, A., Kuswardani, A., Agustiadi, T., and Trenggono, M. (2021). Satellite-observed multi-scale variability of sea surface chlorophyll-a concentration along the south coast of the Sumatra-Java islands. Remote Sensing, 13, 2817. https://doi.org/10.3390/rs13142817

Zhang, L. Y., Du, Y., Cai, W., Chen, Z., Tozuka, T., and Yu, J. Y. (2020). Triggering the Indian Ocean Dipole from the southern hemisphere. Geophysical Research Letters, 47(15), e2020GL088648.

Geophysical Research Letters

Supporting Information for

Can coastal upwelling trigger a climate mode? A study on intraseasonal-scale coastal upwelling off Java and the Indian Ocean Dipole

Takanori Horii[1], Eko Siswanto[2], Iskhaq Iskandar[3], Iwao Ueki[1], and Kentaro Ando[1]

1. Global Ocean Observation Research Center, Research Institute for Global Change, Japan Agency for Marine-Earth Science and Technology, 2-15, Natsushima, Yokosuka, Kanagawa 237-0061 Japan

2. Earth Surface System Research Center, Research Institute for Global Change, Japan Agency for Marine-Earth Science and Technology, 3173-25, Showa-machi, Kanazawa, Yokohama, Kanagawa 236-0001, Japan

3. Faculty of Mathematics and Natural Sciences, Sriwijaya University, Jl. Masjid Al Gazali, Bukit Lama, Palembang 30128, Indonesia

Contents of this file

Text S1 to S2
Tables S1
Figures S1 to S4

Introduction

This Supporting Information contains text, a table, and figures that provide additional information to support the descriptions and analyses in the article.

Satellite-based Chl-a data contain missing values, and the error estimate is essential in creating a proxy for the coastal upwelling along the southern coast of Java. Text S1 describes a method for estimating the error range of the average Chl-a.

Text S2 describes the procedure for decomposing the surface temperature advection (Section 4) into climatological and anomalous components.

Table S1 and Figures S1–4 are supplementary materials cited in the main text and this Supporting Information.

Text S1.

In order to quantify the influence of missing values in calculating the average Chl-a (Figure S1), a proxy of the coastal upwelling along the southern coast of Java, we conducted a statistical experiment using processed Chl-a data (1/8°×1/8°) in 2019 (a pIOD year). In 2019, many observations were obtained without missing values. In the experiment, we prepared multiple Chl-a distributions by superimposing missing-value distributions on the actual snapshots that originally did not contain a missing value in the target area. Then, we evaluated multiple data to estimate the error range of area-averaged Chl-a as follows.

In 2019, the number of days when we were able to observe the area south of Java without a missing value was 160 days. For the period from April to October 2019, the average observation rate was 99.3%.

First, we prepared 492, 605, and 909 snapshots, the data acquisition rates of which were 75%, 50%, and 25%, respectively, based on the actual Chl-a snapshots during 2003–2020 (Figure S2a). For example, for the 605 examples in which both the observed and missing values are 50%, we adopted snapshots with 40% to 60% observed values. Then, we randomly increased or decreased the boundary between the observed and missing values (in other words, increased or decreased the clouds) to adjust the rate to 50%. We did the same for the cases of 75% and 25%.

Second, we used the processed multiple snapshots as a spatial filter with the distribution of 1/NaN, where "1" and "NaN" denote observations and missing values, respectively. We randomly selected the multiple 1/NaN distributions and applied them to the 2019 Chl-a observation data south of Java, and prepared a 365-day timeseries. This procedure was repeated 1,000 times. Thus, we artificially prepared "cloudy" conditions and tested how many observations would be needed to reproduce the Chl-a-based proxy of the coastal upwelling signals.

Using the 1,000 timeseries, we estimated the error range of average Chl-a, which depends on the observation rate and average Chl-a amplitude. Figure S2b shows an example of the one standard deviation based on the 1,000 Chl-a timeseries assuming the observation rates of 50%. We estimated the relationship (ratio) between the original Chl-a amplitude and the standard deviation from the 1,000 timeseries by least-squares fitting, based only on the 160 days without a missing value. The standard deviation increased linearly as the observation rate decreased from 75%, 50%, to 25% (figure not shown). We estimated the error range according to the actual observation rate (0% to 100%) from this relationship. Finally, the error range of average Chl-a timeseries south of Java during 2003–2020 was estimated from the average Chl-a amplitudes and the observation rates for the region south of Java.

We also conducted a second experiment in which we randomly prepared 75%, 50%, and 25% snapshots from the Chl-a data during 2003–2020, reflecting only the probability distribution of the observations. However, this must not be natural because synoptic-scale clouds south of Java are distributed on a spatial scale of several hundred kilometers (Fig. S2a). The results of the second experiment were not conservative. Therefore, in the present study, the results in the first experiment were considered as error ranges in the Chl-a timeseries.

The error range at the first Chl-a blooming in each year is shown in Figure S3. In the error range shown here, the observation error of satellite-observed Chl-a data (0.12 mg/m^3; Xu et al., 2021) was also added.

Text S2.

In order to calculate the horizontal advection of ocean mixed-layer temperature for the diagnosis of temperature balance in the southeastern Indian Ocean (Section 4), we used two satellite-based datasets. Sea surface temperature (SST) data were provided from the National Oceanic and Atmospheric Administration (NOAA) daily optimum interpolation (OI) SST dataset on a 0.25°×0.25° grid (Reynolds et al. 2007). Ocean surface current data were the Ocean Surface Current Analysis-Real Time (OSCAR) data on a 1/3°×1/3 grid (Bonjean and Largerloef, 2002). Since there were several missing values in the coastal area before 2003, we focused on the period of 2003–2020. We re-gridded the SST data onto an OSCAR grid, and horizontal temperature advection was calculated using current velocity and temperature gradient (central differences). This assumes that the SST gradient and OSCAR velocities are representatives of the horizontal gradient and velocity of the ocean mixed layer, respectively. The validity of the calculation was evaluated in our previous studies (Horii et al. 2013).

We calculated the advection terms as daily time steps. The OSCAR data were interpolated from the original data in steps of five to six days to obtain daily values by the spline method.

The climatologies (mean seasonal cycle) and anomalies of SST, surface current, and horizontal temperature advection were calculated using the following procedures. First, based on the 2003–2020 timeseries, the annual cycle and the first three harmonics were estimated by least-squares fitting and were used as the mean seasonal cycle (climatologies). Anomalies are defined as the deviation from the mean seasonal variation.

In order to understand how anomalous temperature advections occurred with the coastal upwelling south of Java, the surface currents and horizontal temperature gradients were decomposed to the following expressions:

$$U = \langle U \rangle + U', \quad V = \langle V \rangle + V', \quad T = \langle T \rangle + T',$$

where the angled brackets denote the mean seasonal cycle (climatology) and the prime denotes the anomalies. The zonal and meridional advections can be decomposed as

$$U T_x = \langle U \rangle \langle T_x \rangle + \langle U \rangle T_x' + U' \langle T_x \rangle + U' T_x' \quad (1)$$

$$V T_y = \langle V \rangle \langle T_y \rangle + \langle V \rangle T_y' + V' \langle T_y \rangle + V' T_y' \quad (2).$$

In the right-hand sides of equations (1) and (2), the terms $\langle U \rangle \langle T_x \rangle$ and $\langle V \rangle \langle T_y \rangle$ represent the climatological temperature advections and the other terms are the anomalies. The terms $U' T_x'$ and $V' T_y'$ are the nonlinear advection terms described in Section 4 (Figure S4).

Table S1. List of year, IOD condition during July–October, date of first Chl-a blooming, and data availability during April–September. The IOD condition was defined as ±0.5 of the average Dipole Mode Index (DMI). The date shows the first significant Chl-a signal exceeding 0.45 (two standard deviations of Chl-a variability from April to June).

Year	IOD	Date: The first Chl-a blooming	Available Chl-a data (April–September)
2003	pIOD	June 8, 2003	95.1 %
2004	Neutral	June 13, 2004	91.2 %
2005	nIOD	July 19, 2005	91.2 %
2006	pIOD	June 7, 2006	93.7 %
2007	pIOD	June 8, 2007	94.7 %
2008	pIOD	May 22, 2008	91.9 %
2009	Neutral	June 29, 2009	91.3 %
2010	nIOD	June 27, 2010	75.6 %
2011	pIOD	June 3, 2011	86.5 %
2012	pIOD	May 24, 2012	97.0 %
2013	Neutral	July 15, 2013	85.9 %
2014	Neutral	August 11, 2014	87.4 %
2015	pIOD	May 14, 2015	92.4 %
2016	nIOD	N/A	86.7 %
2017	pIOD	May 11, 2017	93.2 %
2018	pIOD	May 13, 2018	97.8 %
2019	pIOD	April 24, 2019	99.7 %
2020	Neutral	June 20, 2020	95.5 %

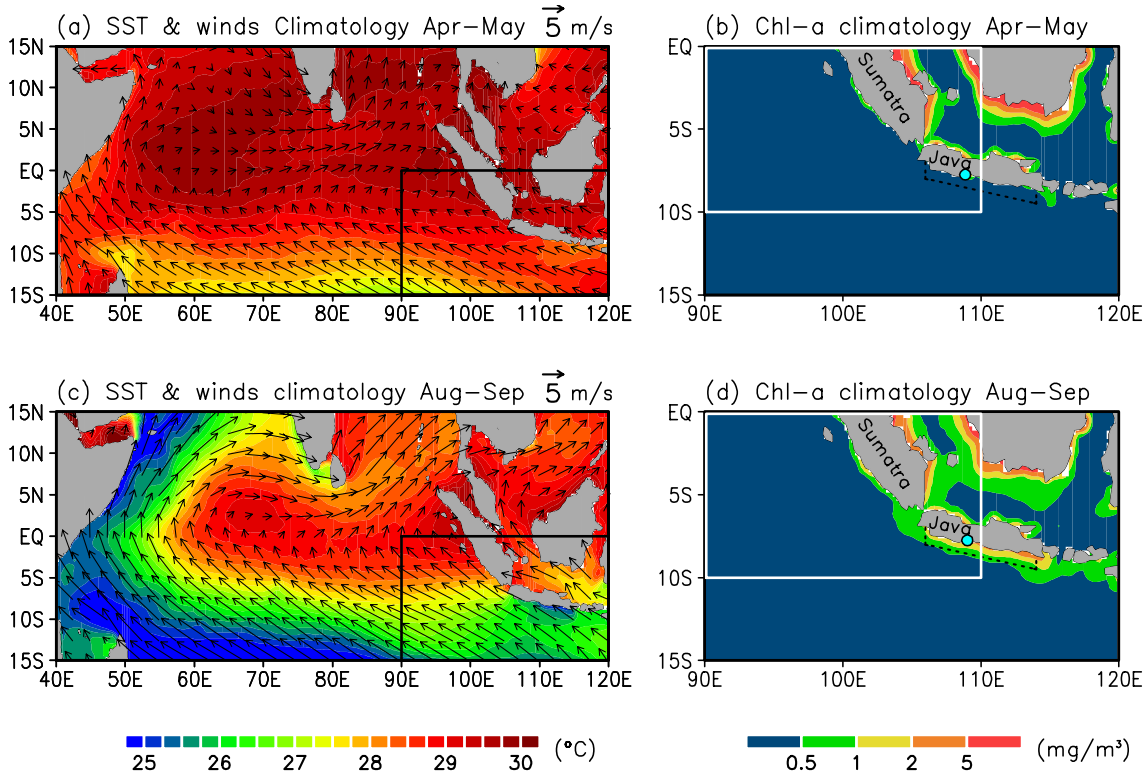

Figure S1. (a) Climatological mean SST and surface winds in April–May. (b) As in (a), but the surface Chl-a concentration for the region 90°E–120°E, 15°S–0° (inset in Figure 1a). The white square represents the eastern pole (90°E–110°E, 10°S–0°) for the calculation of the Dipole Mode Index (DMI) (Saji et al., 1999). The region enclosed by the black dashed lines south of Java (6.5°S, 106°E)–(9.0°S, 114°E) shows the area for the average of Chl-a concentration. A light-blue circle at 7.8°S, 109°E indicates the location of Indonesian tidal station. (c) and (d) As in (a) and (b), respectively, but in August–September.

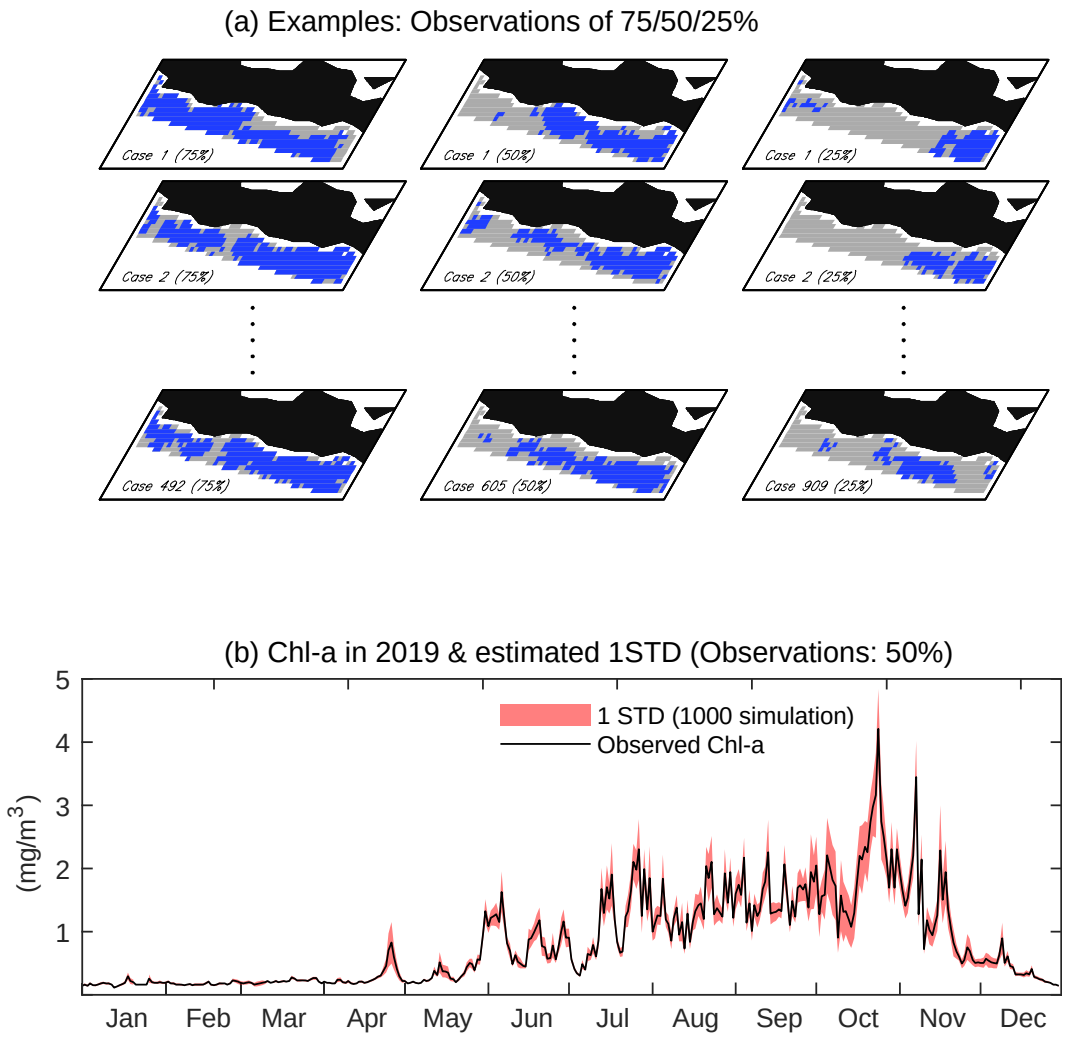

Figure S2. (a) Examples of snapshots with observed and missing values. Blue (gray) grids denote observed (missing) data. Left, middle, and right columns show observed (missing) data of 75% (25%), 50% (50%), and 25% (75%), respectively. The numbers of snapshots during 2003–2020 are 492, 605, and 909, respectively. (b) Timeseries of chlorophyll-a (Chl-a) concentration (mg/m^3) averaged for the region south of Java (see Figure S1 for the map). The light red shading indicates one standard deviation based on simulated 1,000 timeseries using spatial filters in which both the observed and missing values are 50% (see Text S1 for the details).

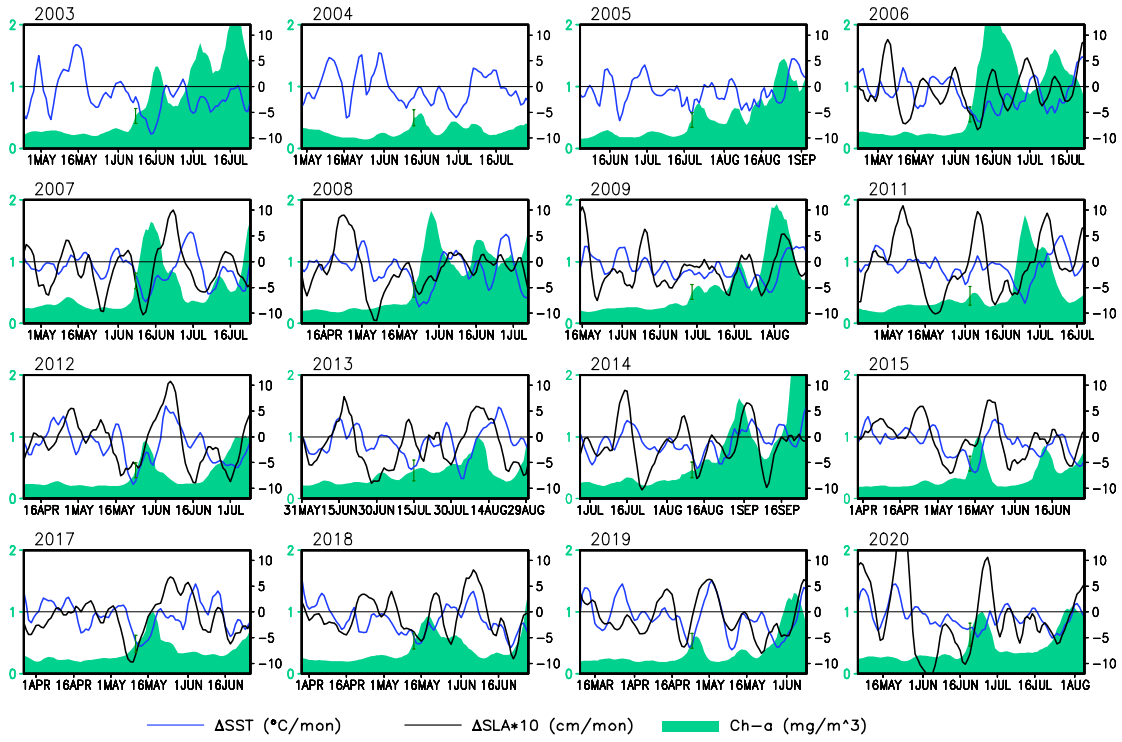

Figure S3. Timeseries of Chl-a concentration south of Java (green shading; mg/m^3; left axis), temporal changes of SSTA (blue; °C/month; right axis) and SLA (black; ×10 cm/month; right axis). The SSTA was averaged for the same region as the Ch-a. A five-day running mean filter was applied to the data. The timeseries show from day −30 to day +30 centered on the first Chl-a blooming of each year. Data for 2010 and 2016 are omitted due to the small amplitudes of Chl-a.

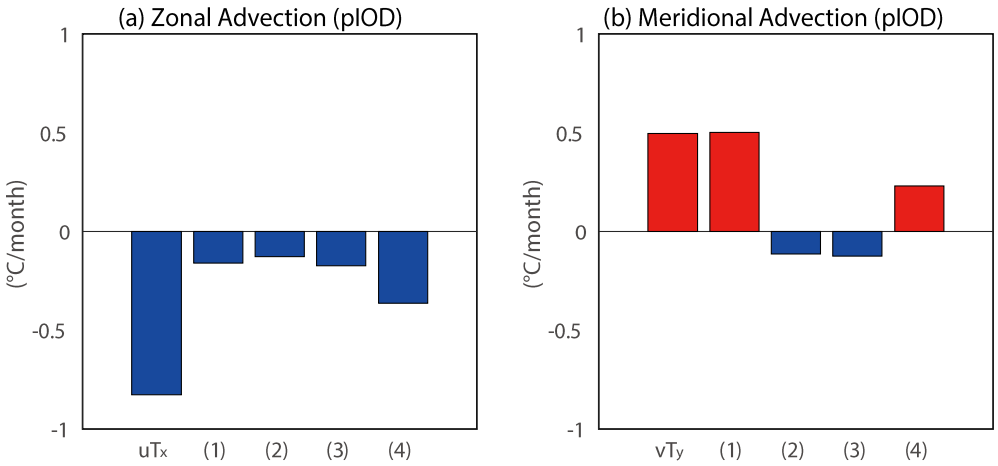

Figure S4. Composite surface temperature advection terms for (a) zonal and (b) meridional components from day 0 to day +30 based on the first coastal upwelling signals for 10 pIOD years. The temperature advection ($u\,T_x$) is decomposed to the climatologies and anomalies as (1) $\langle u \rangle \langle T_x \rangle$, (2) $\langle u \rangle\, T_x'$, (3) $u' \langle T_x \rangle$, and (4) $u'\, T_x'$, respectively, where u (T_x) denotes the zonal surface current (temperature gradient), brackets denote the climatologies, and primes indicate anomalies. The meridional components ($v\,T_y$) are shown in the same way. Positive (negative) values indicate warming (cooling) of the area (100°E–110°E, 10°S–5°S) described in Section 4 and Figure 4.